Model-free control-based vector control of synchronous reluctance motor

Belkacem Selma, Elhadj Bounadja, Bachir Belmadani, Boumediene Selma, Hassane Abouaïssa

Model-free control-based vector control of synchronous reluctance motor

Belkacem Selma[1], Elhadj Bounadja[1], Bachir Belmadani[1],
Boumediene Selma[2], Hassane Abouaïssa[3]

[1] Electrical Engineering Department,
Laboratory of Electrical Engineering and Renewable Energies LGEER
Hassiba Benbouali University of Chlef, 02000 Ouled Farès, Algeria

[2] Higher School of Agronomy, 27000 Mostaganem, Algeria

[3] Univ. Artois, UR 3926, Laboratoire de Génie Informatique
et d'Automatique de l'Artois (LGI2A)
Technoparc Futura
F-62400, Béthune, France

Abstract

The capacity to determine how the state variable system would behave during fixed-point and transition operations is a significant enhancement of the model-free control technique. This paper describes a vector control, also called field-oriented control (FOC) based on model-free control approach for a synchronous reluctance motor (SynRM). The high performance of the proposed model-free control (MFC)-based vector control of SynRM drive is evaluated and compared with (FOC) based on classical proportional–integral (PI) controller under diverse conditions. At last, the results reveal the suggested MFC's efficiency and technical advantages, as well as its advantages over the classical PI.

keyword:
Synchronous reluctance motor (SynRM), Vector control, model-free control (MFC), Classical proportional-integral (PI)

1 Introduction

The synchronous reluctance motors (SynRMs) have recently attracted a lot of attention across a wide range of industrial applications owing to its small size, lower cost, high reliability, high overload ability, high dynamic, great reliability and high power density [1–6]. Furthermore, the SynRMs are seen as a better alternative to induction motors and permanent magnet synchronous motors for many applications, such as fans, washing machines and electric vehicles. Additionally, owing to the absence of the winding and permanent magnet in the rotor, it exhibits a higher energy efficiency, lower rotor temperatures, field-weakening capability, simple manufacturing process and lower overall cost [7–14].

Most industrial applications require high performance, fast transient response and appropriate control flexibility of electric motor drives [15]. It is therefore important to con- duct research on the potential of the SynRMs and their control which remains a challenging task. Both field-oriented con- trol (FOC) and direct torque control (DTC) are two control techniques

that have been widely investigated for SynRM [16–18]. In particular, FOC, also known as vector control, has been widely used in electric drive systems, due to its good performance under both steady-state and transient operating conditions [19, 20]. Vector control technology has resulted in a classic control scheme that is broadly used in the electric drive industry [21]. Depending on whether decoupling is required, vector control techniques can be further arranged into FOC, DTC, etc. [22]. Currently, in the traditional SynRM speed regulation system, the proportional–integral (PI) con- troller is typically employed to set the speed, with a simple algorithm and flexible parameters. Nevertheless, SynRM is a complex research target. Its nonlinearity, multi-objectivity, high coupling and other characteristics show how complicated it is. As a result, under all of these machines' operating conditions, traditional control techniques such as FOC based on PI controllers are unable to provide excellent performance.

2 Literature review

Many control methods applied to the SynRM have been pro- posed in the literature; for example, in [23], the authors have presented a fuzzy sliding mode speed control design procedure for robust stabilization and disturbance rejection of the SynRM drive system. An adaptive nonsingular terminal sliding mode control scheme for SynRM drive system to improve the dynamic performance and robustness has proposed in [24]. In [25], an intelligent maximum torque per ampere tracking control of SynRM using a recurrent Legendre fuzzy neural network is proposed. The authors of [26] have presented an improved model-free predictive current control method for synchronous reluctance motor. A novel Hermite neural network-based second-order sliding mode control method for the synchronous reluctance motor (SynRM) drive system is proposed in [27]. In [28], an artificial neural network is employed as an adaptive solution for reducing the torque ripple in a non-sinusoidal synchronous reluctance motor. The authors of [29] have proposed an intelligent backstepping control using recurrent feature selection fuzzy neural network to construct a high-performance SynRM position servo drive system. A nonlinear backstepping control of SynRM drive system for position tracking of periodic reference inputs with torque ripple consideration is proposed in [30]. In [31], an adaptive backstepping sliding mode control is used to suppress the chaotic oscillations in the SynRM with load vibration perturbation. The authors of [32] have used a flatness-based adaptive neuro- fuzzy control of SynRM with output feedback. A nonlinear controller based on feedback linearization has been designed for SynRM drives that takes into consideration the self- and cross-saturation effects is proposed in [33]. In [34], a non- linear advanced strategy of speed predictive control based on the finite control set model predictive control is proposed for nonlinear SynRMs. An adaptive inductance estimation technique for vector-controlled SynRM drive is presented in [35]. In [36] similar to [34], a finite control set model predictive control method has been developed to improve the performance of a SynRM drive. The authors of [37] have presented model predictive control of SynRM drive configured in open-end winding.

3 Contributions

SynRMs constitute a promising choice for many applications. However, SynRMs have a complicated structure, which affects the control system, and its model is strongly nonlinear. Therefore, conventional control, such as FOC based on PI controller, cannot accomplish high performance for all operating conditions of these modern machines. In addition, traditional vector control structures with PI regulator have some drawbacks such as difficulties in parameter tuning, poor dynamic performances and reduced robustness. In order to avoid difficult mathematical mod-

eling, MFC is suggested as an alternative to classical control. MFC is an algorithm dedicated to systems with poor modeling knowledge. In this paper, FOC is implemented to formulate the dynamic equations. Then, a control principle called model-free control (MFC), which is easy to implement, has been proposed to address the limitations of the conventional control methods. MFC uses a local linear approximation of the process model, which is only valid for a short period of time via the unique knowledge of the input–output behavior, without the need of any mathematical model; then, a fast and simple parameter estimation technique is employed to update the approximation in real time. The main advantage of MFC is that it does not require the process model in the controller tuning. This paper introduces MFC development to control both torque and speed control of SynRM. To verify the advantages of MFC, simulations were carried out under several conditions. Model-free control (MFC) in particular is an interesting alternative; its main advantage is that the controller may be tuned without using a process model [38]. This paper shows how MFC for field-oriented control (FOC) improves the performance of motor drives. It presents three-phase synchronous reluctance motor (SynRM) model in Sect. 2. Section 3 explains how the vector control is used to control the speed and enhance the performance of the SynRM. On the other hand, Section 4 provides an overview of model- free control. Besides, the vector control applied using MFC of SynRM is mentioned in Sect. 5. Furthermore, the implementation in the MATLAB/Simulink environment and its simulation results are given in Section 6 to demonstrate and compare classic PI and intelligent PI. Finally. conclusions and references are cited in the last section.

4 The model of SynRM

The model of the SynRM is presented in a rotating d, q frame. The tension in the synchronous reference frame in SynRM is as follows [39]:

$$\begin{cases} V_{ds} = & R_s i_{ds} + L_d \frac{d}{dt} i_{ds} - \omega_r L_q i_{qs} \\ V_{qs} = & R_s i_{qs} + L_q \frac{d}{dt} i_{qs} - \omega_r L_d i_{ds} \end{cases} \tag{1}$$

where V_{ds} and V_{qs} represent the $dq-$axis stator voltage, R_s is the nominal value of the stator resistance, i_{ds} and i_{qs} represent the $dq-$axis stator current, L_d and L_q are the nominal values of the $dq-$axis inductance of the stator, and ω_r represents the electrical angular velocity of the rotor, respectively.

The electromagnetic torque term is given by [39]:

$$T_e = \frac{3}{2} p \left(\left(L_d - L_q \right) i_{ds} i_{qs} \right) \tag{2}$$

On the other hand, the mechanical equation of the SynRM is given by:

$$J_m \frac{d}{dt} \omega_r = p T_e - p T_r - f_m \omega_r \tag{3}$$

where T_e represents the electromagnetic torque of the motor, p is the number of motor poles, T_r represents the mechanical load torque applied, f_m is the nominal value of the damping coefficient and J_m represents the rotor inertia. These sets of equations characterize the electromechanical behavior of the SynRM.

SynRM's voltage equations are implemented in MATLAB/Simulink environment block, as shown in Fig. 1, using the parameters in Table 1.

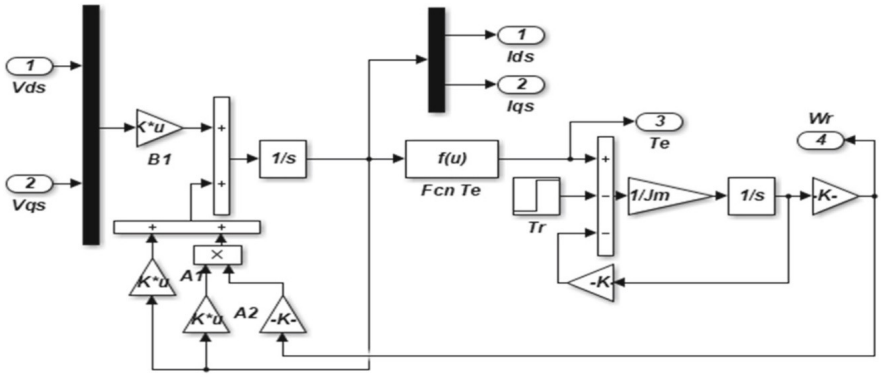

Figure 1: Representation of the SynRM

Table 1: Parameters of SynRM

Symbol	Value
R_s	7.8 Ohm.
L_d	0.4 H
L_q	0.08 H
p	2 poles.
J_m	0.038 Kgm^2

5 FOC of SynRM

The purpose of SynRM vector control is to achieve a model equivalent to the separately excited direct current machine, i.e., a linear and decoupled model that allow to improve their dynamic behavior [40].

The efficiency of motor control is highly dependent on precise knowledge of the mathematical model chosen for the motor and its parameters. In the case of SynRM drives, the Park reference frame is adopted because it is widely used in control and command techniques.

In order to benefit from the highest efficiency of the motor, at speeds below the rated speed, the flux of the motor is chosen so that the current flowing in the stator has the highest torque [39].

By fixing the current ids, the torque according to (2) becomes a linear function of the current i_{qs}; then, the shape of the electromagnetic torque becomes:

$$T_e = \frac{3}{2} p \left(\left(L_d - L_q \right) i_{ds}^{\star} i_{qs} \right) \tag{4}$$

where $i_{ds}^{\star}$ is the constant current i_{ds}.

The quantities $\frac{3}{2} p \left(L_d - L_q \right) i_{ds}^{\star}$ are constant, and the torque is directly proportional to i_q, and hence the following representation:

$$T_e = A i_{qs} \tag{5}$$

with:

$$A = \frac{3}{2} p \left(L_d - L_q \right) i_{ds}^{\star} \tag{6}$$

The system representation of SynRM vector control is shown in Fig. 2.

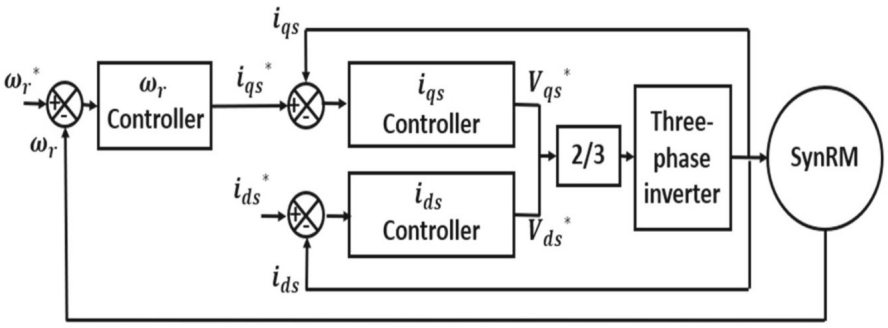

Figure 2: FOC of the SynRM

6 Model-free control

The idea of model-free control for control system applications was originally proposed by Fliess et al. [38, 41]. As technology has evolved, many industrial applications have changed significantly and become more complex. As a result, it becomes very difficult or at least time-consuming to model the dynamics and flows of these applications with mathematical models. In this case, it is not possible to use model-dependent methods for such applications. Instead, MFC uses only online data obtained from the plant to design the controller without any additional information about the mathematical model or the plant parameters being studied. Therefore, MFC is suitable for all nonlinear systems with complex or unknown structures.

6.1 Principle of the method

Consider a physical system governed by an unknown differential Eq. (7) describing the input–output behavior, assumed to be finite-dimensional linear or not and to be well approximated within its operating range,

$$E\left(y, \dot{y}, \ldots, y^{(a)}, u, \dot{u}, \ldots, u^{(b)}\right) = 0 \tag{7}$$

where E is a sufficiently smooth function of its arguments. Suppose that for an integer ν, $0 < \nu \leqslant a$, we have $\frac{\partial E}{\partial y^{(\nu)}} \neq 0$. The control input is denoted by u and the output is denoted by y. The implicit function theorem allows us to locally rewrite (7) in the form

$$y^{(\nu)} = \mathbb{Q}\left(y, \ldots, y^{(\nu-1)}, y^{(\nu+1)}, u, \ldots, u^{(b)}\right) = 0 \tag{8}$$

The idea of the model-free control presented in this article consists in substituting the model (8) by a "phenomenological" model, valid over a short period of time Δ_t.

By setting $\mathbb{Q} = F + \alpha u$, (8) becomes

$$y^{(\nu)} = F + \alpha u, \tag{9}$$

where

- $\alpha \in \mathbb{R}$ is non-physical constant parameter chosen by the practitioner so that F and αu have the same amplitude,

- u and y represent the input and output of the system, respectively,
- $F = y^{(\nu)} - \alpha u$, which is updated, subsumes not only the unmodeled dynamics, but also all the unknown signals (disturbances, noise),
- ν is the order derivative chosen by the practitioner. It can be arbitrarily chosen.

Remark 6.1. *The order of derivation is not necessarily equal to the order of derivation of in (7). In general, we choose equal to 1 or 2.*

The designer must choose the value of the order ν, carefully, taking into account the order of the controlled system and the structure of the feedback control input. Otherwise, the stability of the system may be deteriorated. In several existing examples, M. Fliess and C. Join indicate that ν may always be chosen quite, i.e., 1 [42–47] or 2 [48], and 1 in all concrete situations. For instance, intelligent PID (iPID) is designed with $\nu = 2$, while intelligent PI (iPI) is used with $\nu = 1$.

6.2 Estimation of F

6.2.1 First method

The quantity F in Eq. (9) from the measurement of the output to knowing input [48, 49] is updated at every sampling time. At sampling time k (that is, $t = kT_s$, where T_s is the sampling period), the estimated result of F.

$$\hat{F}(k) = \hat{y}^{(\nu)}(k) - \alpha u(k-1), \tag{10}$$

where $\hat{F}$ is the estimated of F, $\hat{y}^{(\nu)}(k)$ is the estimated of $y^{(\nu)}$ at the time k and $u(k-1)$ is the control input applied to the system during the previous sample period.

6.2.2 Second method

Take the equation of the ultra-local model with $\nu = 2$, for example,

$$\ddot{y}(t) = F(t) + \alpha u(t) \tag{11}$$

Consider the ultra-local model (11). According to a classic result of mathematical analysis, F may be approximated, under a weak integrability condition, by a piecewise constant function. Replace therefore Eq. (11) by

$$\ddot{y} = \Phi + \alpha u \tag{12}$$

where Φ is a constant.

From the rules of operational calculus, Eq. (12) reads

$$s^2 Y - sy(0) - \dot{y}(0) = \frac{\Phi}{s} + U \tag{13}$$

In order to get rid on the initial conditions, derive both sides of the above equation by $\frac{d}{ds}$

$$\frac{2\Phi}{s^3} = s^2 \frac{d^2Y}{ds^2} + 4s\frac{dY}{ds} + 2Y - \frac{d^2U}{ds^2} \tag{14}$$

Multiplying both sides by s^{-N}, $\geqslant 3$, permits to get rid of positive powers of s, i.e., time derivatives, which are very sensitive to corrupting noises. Negative powers of s correspond to iterated time integrals. Thanks to the correspondence between $\frac{d}{ds}$ and the multiplication by $-t$, we obtain in time domain for $N = 3$

$$\hat{F}(t) = \frac{60}{\tau^5} \int_{t-\tau}^{t} \left(\tau^2 + 6\sigma^2 - 6\tau\sigma\right) y(\sigma) d\sigma - \frac{30\alpha}{\tau^5} \int_{t-\tau}^{t} \left(\tau - \sigma^2\right)^2 \sigma^2 u(\sigma) d\sigma \tag{15}$$

According to [50], the robustness with respect to corrupting noise is ensured via the integrals in Eq (15). There is no need to know the precise probabilistic/statistical nature of the noises which are viewed as quick.

Remark 6.2. *Expression* (15) *can be digitally implemented resulting in a FIR filter. For this purpose, the method is modified and we integrate backwards in a small fixed length window T to provide a feasible implementation in real time.*

6.3 Inteligent controllers

6.3.1 Generalities

Consider once more the ultra-local model (9). Close the loop by the intelligent controller

$$u = -\frac{\hat{F} - y^{*(\nu)} + \mathfrak{C}(e)}{\alpha} \tag{16}$$

where

- $y^\star$ is the reference output trajectory,
- $e = y - y^\star$ is the tracking error,
- $\hat{F}$ is an estimated value of F,
- $\mathfrak{C}(e)$ is a causal or unexpected function of e, i.e., $\mathfrak{C}(e)$ depends on the past and present, not on the future. It can be P, PI or PID controller.

The combination of Eqs. (9) and (16) gives the functional equation:

$$e^{(\nu)} + \mathfrak{C}(e) = 0. \tag{17}$$

$\mathfrak{C}$ should be chosen so that correct tracking is guaranteed asymptotically, i.e.,

$$\lim_{t \to \infty} e(t) = 0 \tag{18}$$

Note that $\hat{F}$ does not appear anymore in Eq. (17), i.e., the unknown parts and disturbances of the plant vanish. (When $\hat{F}$ is close enough to F and by combining Eqs. (9) and (16), $F - \hat{F} \simeq 0$). We are therefore left with a linear differential equation with constant coefficients. The tuning of $\mathfrak{C}(e)$ parameters becomes therefore quite straightforward for obtaining a good tracking of $y^\star$. This is a major benefit when compared to the tuning of "classic" PIDs.

The superiority of intelligent controllers, which was already noted in [51, 52], is, however, confirmed:

(1) Tuning the gains of intelligent controllers is s quite simple, whereas it is complex and painful for classic PI or PID controllers.

(2) Contrarily to intelligent controllers, a properly tuned conventional PI or PID controller is unable to take into account heat effects, aging processes, characteristic dispersions due to mass production, etc.

(3) Intelligent controllers handle fault-tolerant control much better than conventional controllers.

This setting is too overall and might not produce tools that are simple to use. The next paragraph fixes this flaw.

6.3.2 Intelligent PIDs

The model-free control law for the system (7) is defined as follows

$$u = u^\star + u_{feedback} \tag{19}$$

where $u_{feedback}$ is a common regulator, such that if $\nu = 1$, $y^{(1)} = F + \alpha u$, we choose $u_{feedback}$ as an PI regulator, if $\nu = 2$, $y^{(2)} = F + \alpha u$, we choose $u_{feedback}$ as an PID regulator, and if $\nu > 2$, we can use generalized proportional–integral regulators (GPIs). The $u^\star$ command is calculated from (19), limited to the case of $\nu = (1, 2)$, when $\nu = 2$, the command (19) can be expressed as follows,

$$u = -\frac{\hat{F} - \ddot{y}^\star + K_P e + K_I \int e + K_D \dot{e}}{\alpha} \tag{20}$$

and when $\nu = 1$

$$u = -\frac{\hat{F} - \dot{y}^\star + K_P e + K_I \int e}{\alpha} \tag{21}$$

where K_P , K_I and K_D are the classic regulator gains.

In the first case, when $\nu = 2$, if $K_I = 0$, we obtain an intelligent proportional derivative controller, or iPD. In the second case, when $\nu = 1$, quite often K_I may be set to 0. It yields an intelligent proportional controller, or iP, quite often encountered in practice. Their lack of any integration of the tracking errors demonstrates that the anti-windup techniques, which are familiar with classical PID and PI controllers, are no more necessary.

Remark 6.3. *The model-free control presented here keeps the simplicity of a classic regulator, in this case a PI. Moreover, the fact of identifying and estimating the internal dynamics of the system endows the controller with a kind of auto-adaptation and robustness, which improves the performance of the control.*

Let us emphasize the following differences with respect to more classic approaches of PID controllers:

- No identification procedure is needed since the whole structural information is contained in the term F (includes not only the unknown structure of the system but also any disturbance). A local linear approximation of the process model can replace the unknown global description of the plant, which is only valid during a short time window. Therefore, it makes it possible to control high-dimensional and/or strongly nonlinear systems without any complex and time-consuming parameter tuning.
- A fast and simple parameter estimation technique, which is employed to update the approximation in real time.

The model-free control schema is described in Fig. 3.

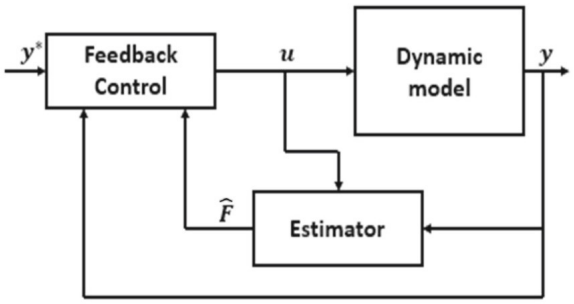

Figure 3: Model-free control scheme

7 Application of model-free control to SynRM Drive

The model-free control presented in the previous section will be applied to a vector control of SynRM. The complex non-linear dynamic model of SynRM can be approximated using an ultra-local model.

7.1 The ultra-local model

Ultra-local model control consists to estimate via only the input and the output signals of non-linear system that can be compensated by control to obtain a good output trajectory tracking effect.

To properly represent the dynamics of SynRM, the ultra- local model in (1) and (3) can be expressed as follows:

$$\begin{cases} \dot{y}_d = \frac{d}{dt} i_{ds} & = F_d + \alpha_d u_d \\ \dot{y}_q = \frac{d}{dt} i_{qs} & = F_q + \alpha_q u_q \end{cases} \tag{22}$$

$$\dot{y}_\omega = \frac{d}{dt}\omega_r = F_\omega + \alpha_\omega u_\omega \tag{23}$$

where

$$y = \begin{bmatrix} i_{ds} \\ i_{qs} \\ \omega_r \end{bmatrix}$$

α_d and α_q represent the scaling factors of D-axis and Q-axis stator input currents, α_ω express the scaling factor of the motor speed, u_d, u_q and u_ω are the system inputs, F_d, $F_d - q$ and F_ω denote the unknown parts including disturbances and uncertainties, and y is the system output.

7.2 Estimation of F

The estimation value of F which is valid during a short lapse of time is evaluated from u and $\dot{y}$ at any time step as follows:

$$\begin{cases} \hat{F}_d(k) = & \dot{y}_d - \alpha_d u_d(k-1) \\ \hat{F}_q(k) = & \dot{y}_q - \alpha_q u_q(k-1) \end{cases} \tag{24}$$

$$\hat{F}_\omega(k) = \dot{y}_\omega - \alpha_\omega u_\omega(k-1) \tag{25}$$

where $\hat{F}_d(k)$, $\hat{F}_q(k)$ and $\hat{F}_\omega(k)$ are the estimated values of F_d, F_q and F_ω, respectively, at time step k, and $u_d(k-1)$, $u_q(k-1)$ and $u_\omega(k-1)$, are the commands at time step $k-1$.

Closing the loop with a linearizing control including a proportional–integral action, we obtain the intelligent proportional–integral controller, or iPI, as described in the following section.

7.3 Model-free control

Based on the ultra-local model, the control law of model-free controller is given as:

$$\begin{cases} u_d = & -\frac{\hat{F}_d - \dot{y}_d^\star + K_{Pd}e + K_{Id}\int e_d}{\alpha_d} \\ u_q = & -\frac{\hat{F}_q - \dot{y}_q^\star + K_{Pq}e + K_{Iq}\int e_q}{\alpha_q} \end{cases} \tag{26}$$

$$u_\omega = -\frac{\hat{F}_\omega - \dot{y}_\omega^\star + K_{P\omega}e + K_{I\omega}\int e_\omega}{\alpha_\omega} \tag{27}$$

where $\hat{F}_d$, $\hat{F}_q$ and $\hat{F}_\omega$ denote the estimated values of F_d, F_q and F_ω, respectively, $\dot{y}_d^\star$, $\dot{y}_q^\star$ and $\dot{y}_\omega^\star$ are the desired output, $e_d = y_d^\star - y_d$, $e_q = y_q^\star - y_q$ and $e_\omega = y_\omega^\star - y_\omega$ are the tracking errors, and K_{Pd}, K_{Id}, K_{Pq}, K_{Iq} and $K_{P\omega}$ and $K_{I\omega}$ are the classic PI tuning gains. It is clear that the tracking performance of system can be accomplished by only tuning K_P and K_I when $\hat{F}$ is well estimated; moreover, the closed-loop model-free controlled nonlinear system stability has been verified [53].

The block diagram of the vector control based on model- free control of a synchronous reluctance motor in this paper is shown in Fig. 4.

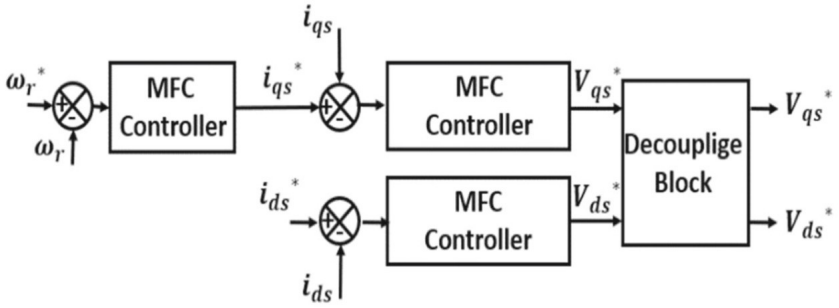

Figure 4: Block diagram of the SynRM vector control with the model-free control

8 Simulation results

The proposed MFC algorithm for the SynRM drive was implemented and simulated under different operation conditions. The control performances obtained with MFC are compared with the performances achieved using conventional PI. The classical PI controller requires knowledge of all machine parameters and its payloads, which may not be realistic. The obtained results with fixed step time $\Delta t = 0.0001s$ are shown below. The simulation conditions are set as fol- lows: The drive response corresponds to a step change on the speed reference from 0 to 1500 rpm, and during $q-axis$ testing, the $d-axis$ command was set to 3 A. Results for the two controllers (PI

and MFC) are shown in Figs. 5, 6, 7 and 8, in which the outputs of the closed-loop system are given. Figure 5 illustrates the evolution of the speed of the SynRM with PI and MFC controllers compared to the desired trajectory. The trajectory of speed with the MFC system (black color) is very close to the desired trajectory (green color). On the other hand, the PI trajectory (red color) of the speed response is satisfactory. We can say the same thing about torque and $dq-axis$ stator current response. For example, Fig. 6 shows that the torque ripple response with MFC controller (black color) is reduced compared to torque (red color) controlled by PI controller, which is with this last one considerable. It was the same for $dq-axis$ current control response curve shown in Figs. 7 and 8, interestingly, note that, during the transient response, both d-axis current and q-axis current tracked the references very well, and there was no steady-state error using MFC. On the other hand, the $dq-axis$ current of the FOC with the PI controller exhibits a considerable overshoot.

PI controller algorithm is simple, but it requires high accuracy in system model and parameters. The simulation results presented in Figs. 5, 6, 7 and 8, show that MFC controller gives good results and the trajectories follow the desired tracks. At $t = 2s$, the load of $10N.m$

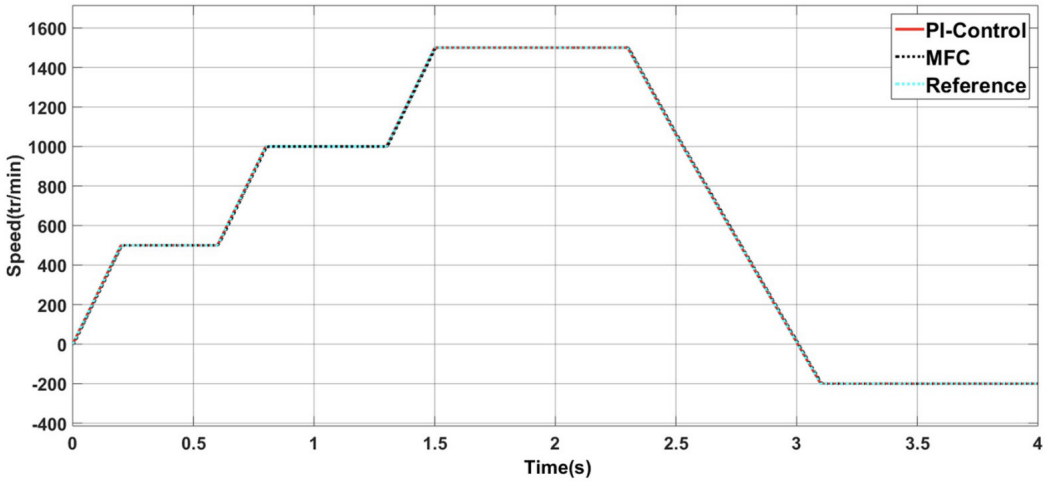

Figure 5: Speed response of motor

has been suddenly applied to the running machine. The reference speed is fixed at 1500 rpm. The simulation conditions are as follows: The speed ranges from 0 to 1500, sudden increase of $10N.m$ on the load torque at 2 s and during q-axis testing, the d-axis command was set to 3 A. Figures 9, 10, 11 and 12 show the high disturbance rejection ability of the MFC applied to the SynRM. Figure 9 shows the speed evolution of the motor, where it is clear that MFC has a good speed trajectory (black color) compared to the reference one (green color) and the trajectory of speed with the MFC system (red color) is very close to the desired trajectory (blue color). On the other hand, the PI speed trajectory (black color) is satisfactory with small overshoot. As a result, the speed control performance was significantly improved, confirming the feasibility of the proposed MFC for this application. MFC allows to avoid the current ripple and to follow correctly the reference trajectory without fluctuation for the d-axis. Note that, under the action of the proposed model-free control, when the load changed suddenly, the q-axis deviated slightly from its set point, but it recovered very quickly, which is clearly not the case with the PI controller; we notice a considerable overshoots on the $dq-axis$ and the torque at the time $t = 0.25s$, when the speed becomes 1500 rpm and at the time when the load is added. Furthermore, large

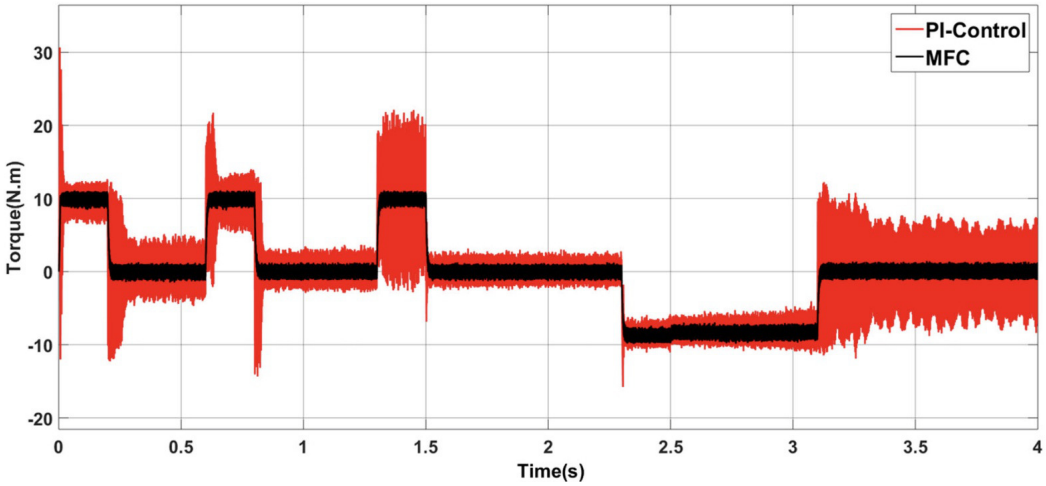

Figure 6: Torque response of motor

fluctuations after $t = 2s$, due to the load. The PI controller is provided to deal with inevitable modeling errors and uncertainties.

Interestingly, the proposed MFC algorithm provided high performance for the SynRM drives compared to FOC with the classical PI controller. In summary, by applying MFC and the corresponding intelligent controllers, the performance of the SynRM was improved in terms of not only the current control but also the speed control. Also, the disturbance rejection capability of the MFC confirms the feasibility of this technique for this application. Moreover, the coefficients of intelligent controllers of the MFC are not complicated to tune, and a simple design approach can be applied for the SynRM drive.

9 Conclusion

In this paper, model-free controller (MFC) is used for speed and current control of motor drives in order to achieve a good speed and current tracking trajectories, solve the problem of model mismatch caused by the change in the motor parameters, and reduce the degradation of control performance caused by the known and unknown disturbances of the motor. This novel control method is applied to the vector control of SynRM to realize the combined control of speed and current control. The simulation results show that the method has fast dynamic response and small fluctuation of engine torque, which has great advantages compared with traditional PI control. Finally, the potential of MFCs demonstrated in this study should inspire further research and analysis of such controllers to gain the necessary expertise to translate the results into practical applications.

References

[1] Moghaddam RR, Gyllensten F (2014) Novel high-performance SynRM design method: an easy approach for a complicated rotor topology. IEEE Trans Industr Electron 61(9):5058–5065

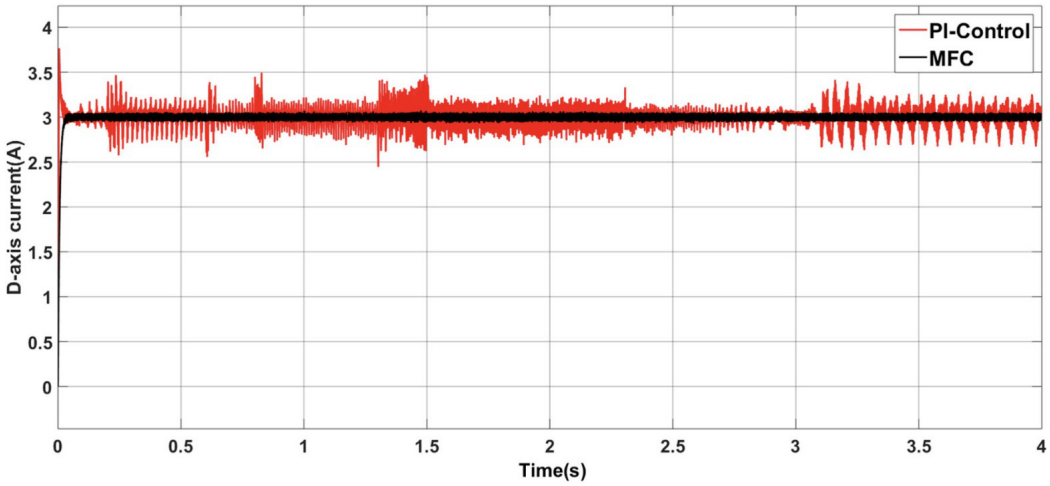

Figure 7: D-axis current

[2] Taghavi SM, Pillay PA (2015) Mechanically robust rotor with trans- verse laminations for a wide-speed-range synchronous reluctance traction motor. Trans Ind Appl 51(6):4404–4414

[3] Ibrahim MNF, Abdel-Khalik AS, Rashad EM, Sergeant P (2018) An improved torque density synchronous reluctance machine with a combined star–delta winding layout winding layout. IEEE Trans Energy Convers 33:1015–1024

[4] Li Z, Bao X (2019) Analysis of vibration and noise of induction motor equipped with concentric single-double-layer star-delta winding. Chin J Electr Eng 5(1):36–46

[5] Reddy MHV, Gowri KS, Reddy TB et al (2019) Effect of center voltage vectors (CVVs) of three-level space plane on the perfor- mance of dual inverter fed open end winding induction motor drive. Chin J Electr Eng 5(2):43–55

[6] Tawfiq KB, Ibrahim MN, El-Kholy EE, Sergeant P (2021) Performance improvement of synchronous reluctance machines—a review research. IEEE Trans 57:1–11

[7] Kolehmainen J (2010) Synchronous reluctance motor with form blocked rotor. Trans Energy Convers 25(2):450–456

[8] Bianchi N, Degano M, Fornasiero E (2013) Sensitivity analysis of torque ripple reduction of synchronous reluctance and interior PM motors. IEEE Trans Ind Appl 51:187–195

[9] De Almeida AT e al (2014) Beyond induction motors-technology trends to move up efficiency. IEEE Trans Ind Appl

[10] Rouhani R, Abdollahi SE, Gholamian SA (2018) Torque ripple reduction of a synchronous reluctance motor for electric vehicle applications. In: 9th annual power electronics, drives systems and technologies conference (PEDSTC), pp 386–391

[11] Ozcelik NG, Dogru UE, Imeryuz M, Ergene LT (2019) Synchronous reluctance motor versus induction motor at low- power industrial applications: design and comparison. Energies 12(11):2190

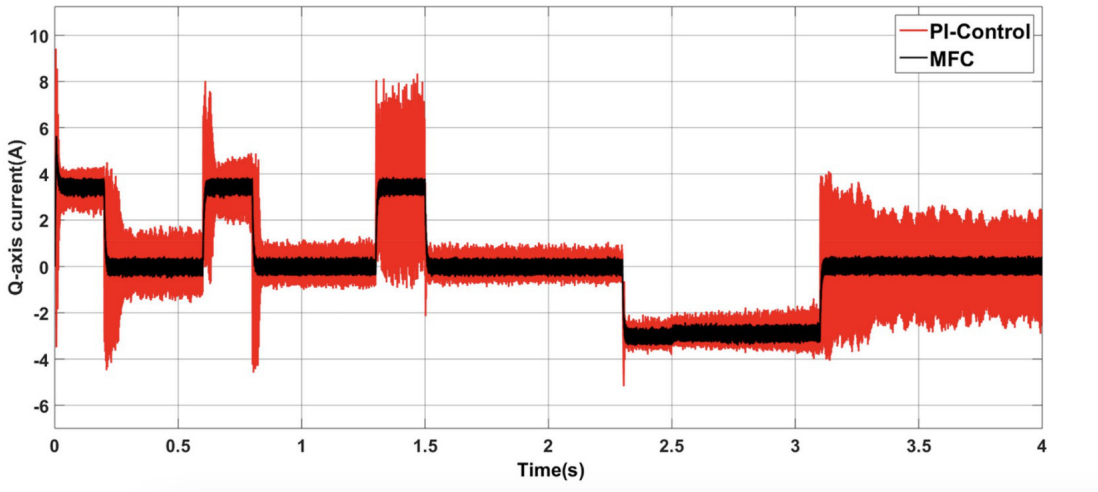

Figure 8: Q-axis current

[12] Zhou M,Zhang X, Zhao W e tal (2019) Influence of magnet shape on the cogging torque of a surface-mounted permanent magnet motor. Chin J Electr Eng 5(4):40–50

[13] Rassõlkin A et al (2020) Life cycle analysis of electrical motor- drive system based on electrical machine type. Proc Est Acad Sci 69(2):162

[14] Villani M, Fabri G, Credo A, Di Leonardo L, Collazzo FP (2022) Line-start Synchronous Reluctance Motor: a reduced Manufacturing cost Avenue to Achieve IE4 Efficiency Class. IEEE Access 10:100094–100103

[15] Finch JW, Giaouris D (2008) Controlled ac electrical drives.Trans Industrial Electron 55(2):481–491

[16] Malekian K, Sharif MR, Milimonfared J (2008) An optimal current vector control for synchronous reluctance motors incorporating field weakening. In: 10th IEEE International workshop on advanced motion control Trento, Italy, vol 8, pp 393–398

[17] Foo GHB, Zhang X (2017) Robust direct torque control of synchronous reluctance motor drives in the field-weakening region. Trans Power Electron 32(2):1289–1298

[18] Zang X, Foo GHB (2018) Over-modulation of constant switch- ing frequency-based DTC for reluctance synchronous motors incorporating field-weakening operation. Trans Industrial Electron 66(1):37–47

[19] Antonello R, Ortombina L, Tinazzi F, Systems D et al (2017) (PEDS), Honolulu, USA, PEDS, pp 1037–1042

[20] Ghosh PR, Das A, Bhuvaneswari G (2017) Performance comparison of different vector control approaches for a synchronous reluctance motor drive. In: IEEE 6th International conference on computer applications in electrical engineering-recent advances (CERA), Roorkee, India, CERA pp 320–325

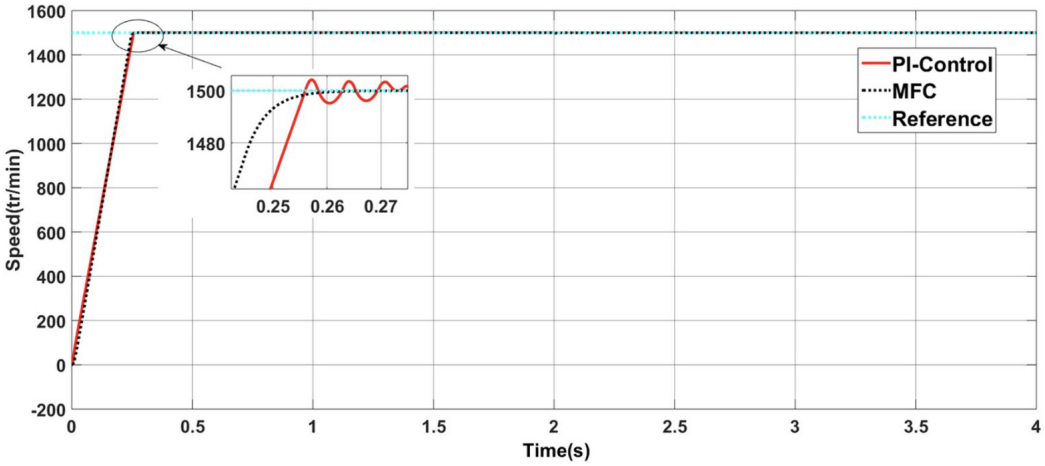

Figure 9: Speed response of motor

[21] Heidari H,Rassolkin A,Kallaste A, Vaimann T, An-driushchenko E (2020) Vector control of synchronous reluctance motor with reduced torque ripples. In: XI international conference on electrical power drive systems (ICEPDS), pp 1–5

[22] Heidari H et al (2021) A review of synchronous reluctance motor- drive advancements. Sustainability 13:729

[23] Chen CA, Chiang HK, Tseng CH (2008) The novel fuzzy sliding mode control of synchronous reluctance motor. In: Eighth international conference on intelligent systems design and applications

[24] Ren L, Lin G, Zhao Y, Liao Z, Peng F (2021) Adaptive nonsingular finite-time terminal sliding mode control for synchronous reluctance motor. IEEE Access 9:51283–51293. https://doi.org/10. 1109/ACCESS.2021.3068745

[25] Lin FJ, Huang MS, Chen SG, Hsu CW (2019) Intelligent maxi- mum torque per ampere tracking control of synchronous reluctance motor using recurrent Legendre fuzzy neural network. IEEE Trans Power Electron 34(12):12080–12094. https://doi.org/10. 1109/TPEL.2019.2906664

[26] Lin CK, Yu JT, Lai YS, Yu HC (2016) Improved model-free predic- tive current control for synchronous reluctance motor drives. IEEE Trans Ind Electron 63(6):3942–3953. https://doi.org/10.1109/TIE. 2016.2527629

[27] Liu YC, Laghrouche S, N'Diaye A, Cirrincione M (2021) Hermite neural network-based second-order sliding-mode control of synchronous reluctance motor drive systems. J Frankl Inst Eng Appl Math 358(7):4118–4119

[28] Truong PH, Flieller D, Nguyen NK, Merclé J, Sturtzer G (2016) Torque ripple minimization in non- sinusoidal synchronous reluctance motors based on artificial neural networks. Electr Power Syst Res. https://doi.org/10.1016/j.epsr.2016.06.045

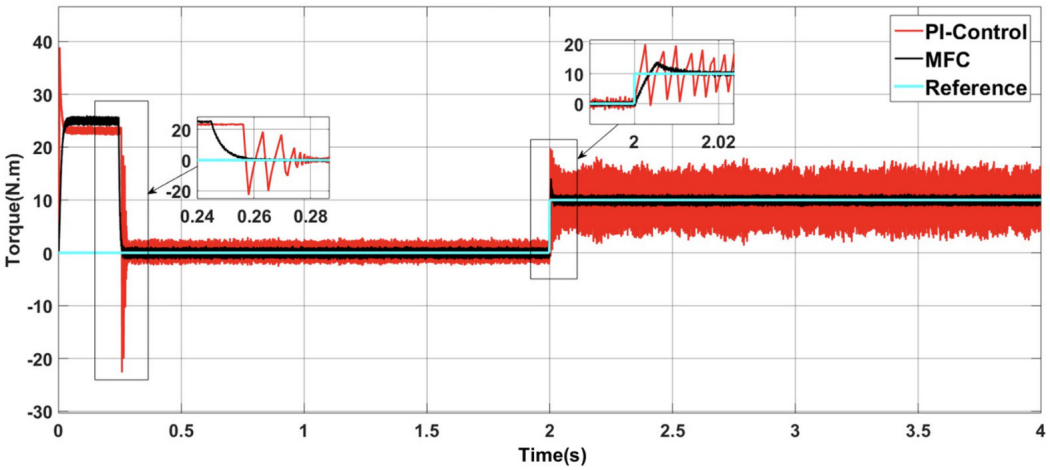

Figure 10: Torque response of motor

[29] Lin FJ, ChenS G, Hsu CW (2019) Intelligent backstepping control using recurrent feature selection fuzzy neural network for syn- chronous reluctance motor position servo drive system. IEEE Trans Fuzzy Syst 27(3):413–427

[30] Lin CH, Ting JC (2019) Novel nonlinear backstepping control of synchronous reluctance motor drive system for position tracking of periodic reference inputs with torque ripple consideration. Int J Control Autom Syst 17:1–17

[31] Kingni ST, Cheukem A, Tuwa PRN et al (2021) Synchronous Reluctance Motor with load vibration perturbation: analysis, electronic implementation and adaptive backstepping sliding Mode Control. Iran J Sci Technol Trans Electr Eng 45:645–654. https://doi.org/10.1007/s40998-020-00390-w

[32] Rigatos G, Siano P, Wira P, Moreno-Munoz A (2018) Flatness based adaptive control of synchronous reluctance machines with output feedback. In: 5th international symposium on environment- friendly energies and applications (EFEA)

[33] Accetta A, Cirrincione M, Pucci M, Sferlazza A (2019) A non-linear control of synchronous reluctance motors (SynRM) based on feedback linearization considering the self and cross-saturation effects. IEEE energy conversion congress and exposition (ECCE)

[34] Farhan A, Abdelrahem M, Hackl CM, Kennel R, Shaltout A, Saleh A (2020) Advanced Strategy of Speed Predictive Control for Non- linear Synchronous Reluctance Motors. Machines 8(3):44

[35] Bhattacharyya R, Basak S, Chakraborty C (2021) An adaptive inductance estimation technique for vector-controlled synchronous reluctance motor drive. In: IEEE 30th International symposium on industrial electronics (ISIE), Kyoto, Japan, pp 1–6

[36] Riccio J, Karamanakos P, Odhano S, Tang M, Nardo MD, Zanchetta P (2021) A direct Model Predictive Control Strategy for High- Performance Synchronous Reluctance Motor drives. IEEE Energy Conversion Congress and Exposition (ECCE), Vancouver, BC, Canada, pp 4704–4710

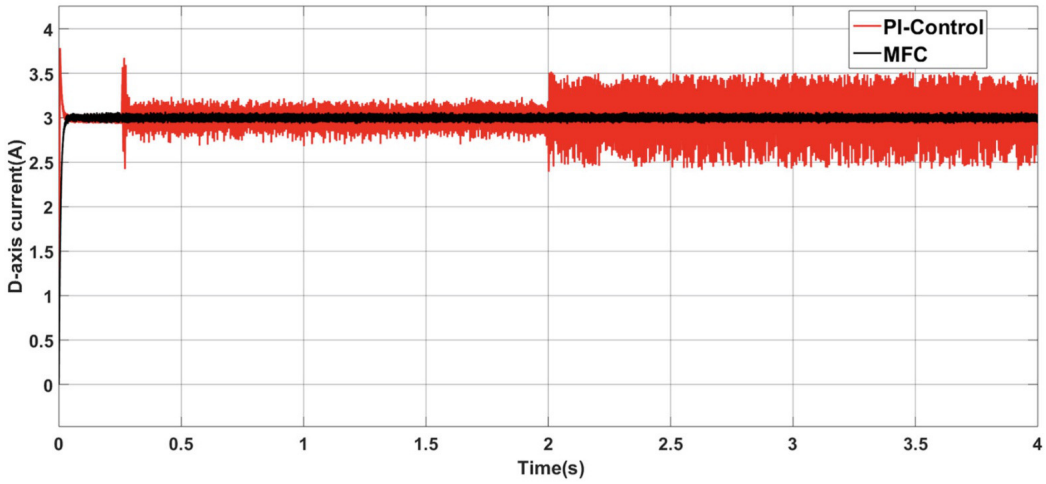

Figure 11: D-axis current

[37] Riccio J, Rovere L, Odhano S, Di Nardo M, Zanchetta P (2022) Model-predictive control of Open-End Winding Synchronous Reluctance Motor drives. IEEE Energy Conversion Congress and Exposition (ECCE), Detroit, MI, USA, pp 1–8

[38] Fliess M, Join C (2013) Model-free control. Int J Control 86:2228–2252

[39] Heidari H et al (2021) A comparison of the vector control of synchronous reluctance motor and permanent magnet-assisted synchronous reluctance motor. XVIII International scientific technical conference alternating current electric drives (ACED), Ekaterin- burg, Russia, pp 1–6 https://doi.org/10.1109/ACED50605.2021. 9462265

[40] Norris JA (1993) Vector control of A.C. motors. IEEE annual tex- tile, fiber and film industry technical conference, pp 1–8

[41] Fliess M, Join C (2014) Stability margins and model-free control: a first look. In Proceedings of the European control conference (ECC), Strasbourg, France, pp 24–27

[42] Wang Z, Zhou X, Wang J (2022) Extremum-Seeking-based adaptive model-free control and its application to automated vehicle path Tracking. IEEE/ASME Trans Mechatron 27(5):3874–3884. https://doi.org/10.1109/TMECH.2022.3146727

[43] Guilloteau Q, Robu B, Join C, Fliess M, Rutten E, Richard O (2022) Model-Free Control for Resource Harvesting in Computing Grids. In: IEEE conference on control technology and applica- tions (CCTA), Trieste, Italy, pp 384–390. https://doi.org/10.1109/CCTA49430.2022.9966035

[44] Michel L, Neunaber I, Mishra R, Braud C, Plestan F, Barbot JP et al (2022) Model-free control of the dynamic lift of a wind turbine blade section: experimental results. J Phys Conf Ser 2265(3):032068

[45] Join C, Fliess M, Chaxel F (2020) Model-free control as a service in the industrial Internet of Things: packet loss and latency issues via preliminary experiments. In: 16th Mediterranean conference on control and automation, Saint-Raphaël

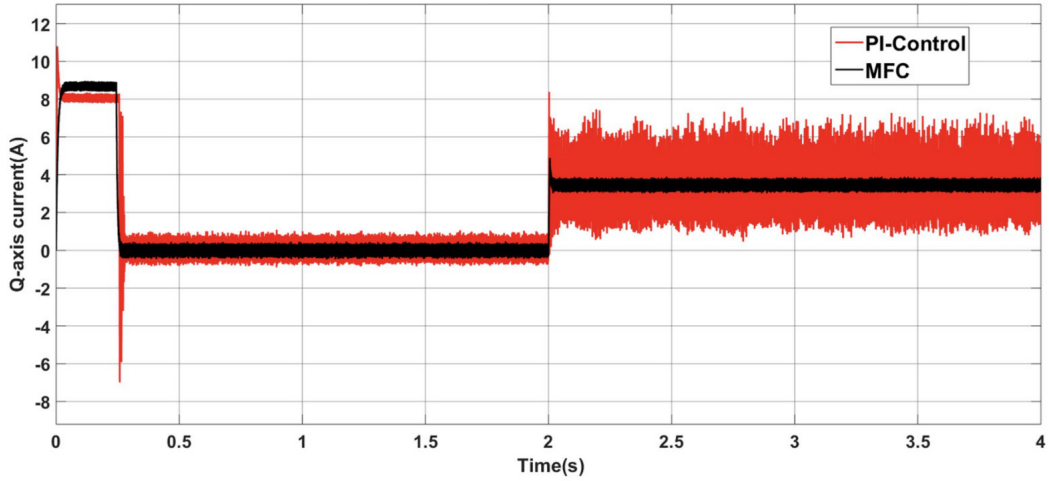

Figure 12: Q-axis current

[46] Lafont F, Balmat JF, Join C, Fliess M (2020) First steps toward a simple but efficient model-free control synthesis for variable-speed wind turbines. Int J Circuits Syst Signal Process 14

[47] Abouaissa H, Fliess M, Join C (2017) On ramp metering: towards a better understanding of ALINEA via model-free control. Int J Control 90(5):1018–1026

[48] Abouaïssa H, Chouraqui S (2019) On the control of robot manipulator: a model-free approach. J Comput Sci 31:6–16

[49] Lafont F, Balmat JF, Pessel N, Fliess M (2015) A model-free control strategy for an experimental greenhouse with an application to fault accommodation. Comput Electron Agric 110:139–149

[50] Fliess M (2006) Analyse non standard du bruit. C R Acad Sci Paris Ser I 342:797–802

[51] Fliess M, Join C (2008) Commande sans modèle et commande à modèle restreint. e-STA 4(5):1–23

[52] Fliess M, Join C (2009) Model-free control and intelligent PID controllers: towards a possible trivialization of nonlinear control?. In: Proceedings of 15th IFAC symposium on system identification, SYSID, Saint-Malo, vol 15, pp 1531–1550

[53] Fliess M, Join C (2014) Stability margins and model-free control: a first look. European Control Conference (ECC), IEEE, New York, pp 454–459